Article

Mechanism Analysis of Delayed Water Inrush from Karst Collapse Column during Roadway Excavation Based on Seepage Transition Theory: A Case Study in PanEr Coal Mine

Yu Liu [1], Jingzhong Zhu [2,*], Qimeng Liu [2], Anying Yuan [1], Shifang He [3] and Yisheng Bai [3]

1 State Key Laboratory of Mining Response and Disaster Prevention and Control in Deep Coal Mines, Anhui University of Science and Technology, Huainan 232001, China; yliu@aust.edu.cn (Y.L.); ayyuan@aust.edu.cn (A.Y.)
2 School of Earth and Environment, Anhui University of Science and Technology, Huainan 232001, China; qmliu@aust.edu.cn
3 Coal Company, Huaihe Energy (Group) Co., Ltd., Huainan 232001, China; heshifang2022@163.com (S.H.); baiyisheng2022@163.com (Y.B.)
* Correspondence: algzjz0801@126.com

Abstract: Water inrush disaster is one of the major disasters affecting the production safety of coal mines following roof caving, fire, gas outburst, and dust explosion disasters. It is urgent to reveal the water inrush mechanism and take effective measures to prevent the disasters. More than 80% of water inrush accidents occur around geological structural zones such as faults and karst collapse columns (KCCs). The water inrush events from KCCs caused huge economic losses and heavy casualties, and the water inrush process often shows certain hysteresis characteristics. Taking the water inrush disaster from a KCC during roadway excavation in PanEr Coal Mine of Huainan Mining Area as the case study, the delayed inrush mechanism of KCC was analyzed from the aspects of floor failure, KCC activation, seepage transition, and water inrush development characteristics. The results show that the rock mechanical properties and the excavation depth are the main factors affecting the floor failure characteristics. The seepage transformation from pore flow to fracture flow and pipeline flow, with the change in internal composition structure, is the internal mechanism of the delayed water inrush from KCC. The research is of great significance for the prediction and prevention of water inrush disasters from KCCs.

Keywords: water inrush; karst collapse column; seepage transition; coal mining

1. Introduction

Karst collapse columns (KCCs) are special geological structures concealed in the limestone strata that are difficult to be found in the exploration before mining activities [1]. The KCC is usually filled with irregular rock blocks collapsed from the overlying strata, with an incomplete structure and developed cracks. Once the mining or excavation affects the KCC connected with the Ordovician limestone aquifer with strong water yield, the high-pressure groundwater penetrates the filling and dramatically flows along the fracture channel. More than 5000 KCCs have been found in 45 mining areas in the Northern China coalfield, mainly distributed in Shandong, Hebei, Shanxi, Anhui, and Henan provinces [2–4]. In recent years, with the increase in excavation depth, the water inrush disasters caused by KCCs have become more and more serious. This has aroused widespread concern, and some studies on the shape, water inrush mode, development, and seepage characteristics were carried out [5,6].

In the early stage, scholars studied the morphological characteristics and pointed out that the cross-sectional morphology was mainly round, oval, and triangular [7–9]. It is usually cylindrical or conical in profile and in serrated contact with the surrounding rocks.

With the improvement of research methods and technologies, the formation mechanism, water inrush characteristics, and water disaster prediction and prevention were analyzed. The controlling factors of paleokarst and KCCs in Huainan Mining Area were considered as strata lithology, limestone crack structure, corrosive fluids, and geological structures [10].

The basic conditions of KCC formation include a soluble rock layer, good groundwater channel, intrusive water, and flowing groundwater. The "thick-walled cylinder" theory was put forward on the basis of the relative position relationship between KCC and stope or roadway, and the water-filled collapse column was simplified into an infinite thick-walled bucket with uniform internal pressure [11]. The formation causes of KCCs were summarized as gravity collapse, gypsum dissolution, vacuum erosion, and hydrothermal origin theory [12–15]. However, there is still no consensus in the understanding of the formation mechanism. Mechanics analyses, numerical simulations, similar material experiments, and in situ monitoring methods were used to analyze the influence of the KCCs on mine pressure distribution during mining [16–18]. Tang et al. proposed that water inrush events of the activated collapse column appeared during the process of rock damage, micro-bur, and macro-fracture formation [19]. The activation of KCCs in the water inrush process went through high-pressure water seepage, erosion, fracture germination, and expansion [20]. The treatment methods after water inrush mainly include physical exploration and drilling grouting [21,22].

The water inrush from KCCs is generally induced by multiple factors, including the downward fractures caused by excavation, the development of collapse column rock cracks, and high water pressure from limestone aquifer. On 25 May 2017, water inrush from a KCC occurred during roadway excavation in the PanEr Coal Mine of Huainan Mining Area. The main cause was the development of a concealed collapse column underneath connecting with Ordovician limestone aquifers. Under the combined action of mining stress and confined water, the groundwater from Ordovician limestone rushed into the roadway.

In this paper, the 25 May water inrush accident was taken as the case study. On the basis of the analysis of the stratum, geological structure, and hydrogeological conditions, the theoretical analysis of floor failure under excavation disturbance was carried out, and the hydraulic criterion of water inrush from the KCC was determined. In addition, the activated hydraulic conductivity of the collapse column was analyzed by numerical simulation, and the seepage transition theory was proposed and further verified by the dynamic change of groundwater inflow. This research is of great significance for the analysis, prediction, and prevention of water inrush disasters from karst collapse columns.

2. Study Area

The PanEr Coal Mine is located within longitudes 116°49′26″ E to 116°51′10″ E and latitudes 32°46′02″ N to 32°50′21″ N in northern Huainan City of Anhui Province of China, as shown in Figure 1a. The ground elevation ranges from 20.5 m to 22 m, and the overall trend is gradually decreasing from northwest to southeast.

The main strata, from old to new, are Ordovician, Carboniferous, Permian, Triassic, Paleogene, Neogene, and Quaternary, as shown in Figure 1b. Group A coal seams at the bottom of Permian system are mainly exploited, including No. 1 and No. 3 coal seams. The geological structure of the PanEr Coal Mine is complex. A total of 413 faults, including one knob fault, 298 normal faults, and 114 reverse faults, are developed in the study area (Figure 1). There are seven faults with a scarp ≥100 m, 18 faults with a scarp ≥50 m, and 74 faults with a scarp ≥20 m. As shown in Figure 1a, 10 main regional faults (F1 to F10) are included in the research area, with F1 and F2 in the E–S direction, F3 to F8 in the E–N direction, F9 (knob fault) in the SE–ES direction, and F10 in the N–E direction. Geological investigation and production exposure showed that the faults are mostly filled with argillaceous materials, with low water content and poor water conductivity. Small-sized faults are relatively developed near or at the intersection of large and medium-sized faults and in tectonic stress concentration areas.
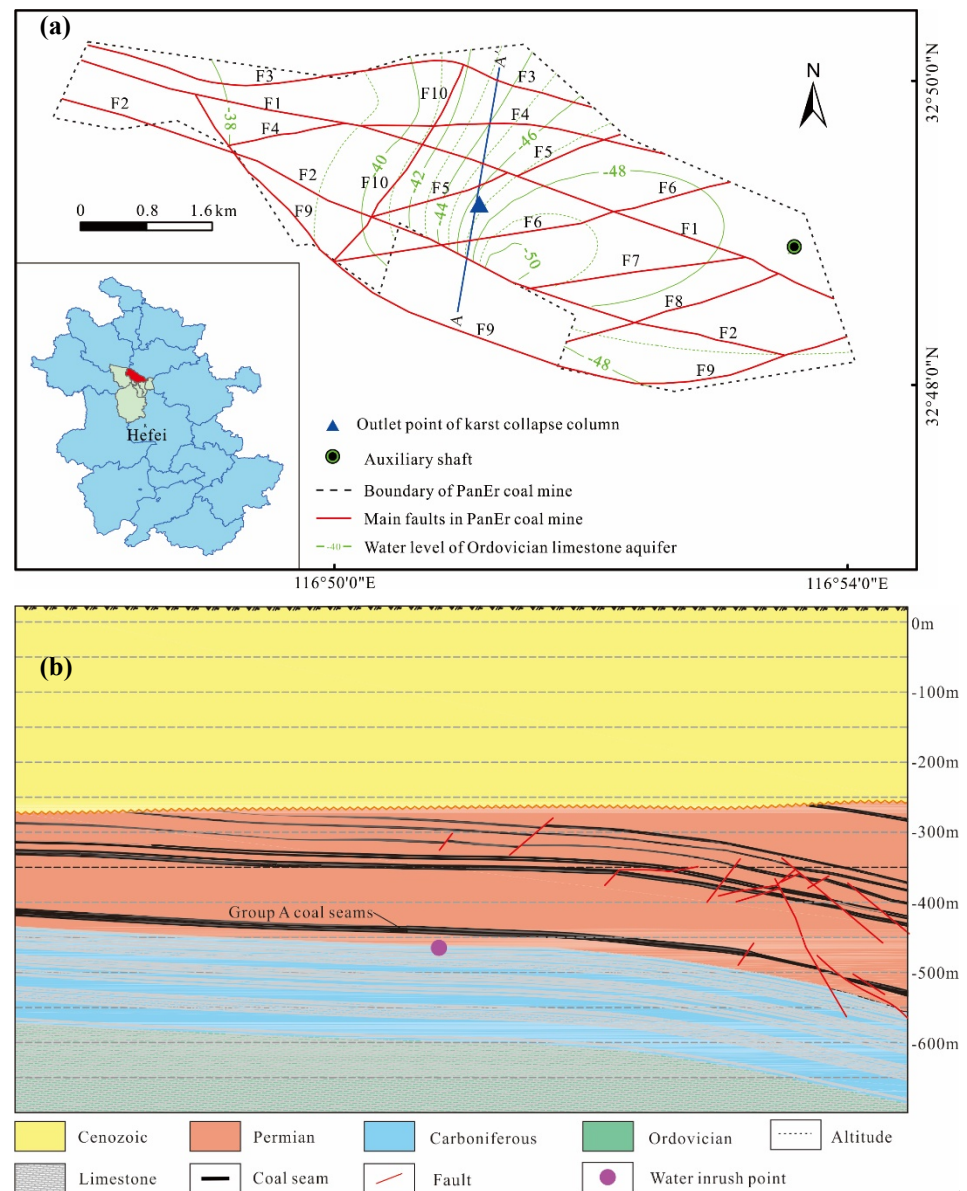
Figure 1. Location, geological plan, and profile of the study area. (**a**) location and geological plan; (**b**) geological profile.

The limestone aquifer of the Carboniferous Taiyuan Formation and the Ordovician have a significant influence on the excavation of group A coal seams. The Taiyuan formation is composed of thin limestone, mudstone, and sandy mudstone. The total thickness is 89.90 m to 140.79 m, with an average of 117.82 m. This formation contains 10 to 12 limestone aquifers, which are divided into three groups, C_3I (No. 1 to No. 3), C_3II (No. 4 to No. 9), and C_3III (No. 10 to No. 12), from top to bottom. The unit water inflow of the aquifers is 0.000009 L/(s·m) to 0.0187 L/(s·m), and the permeability coefficient is 0.0056–0.017 m/day. The Ordovician strata are mainly composed of dolomitic thick limestone, with exposed thickness of 3.22 m to 191.71 m. Their unit water inflow is 0.005509 L/(s·m) to 1.283l L/(s·m), with a permeability coefficient of 0.0526 m/day to 0.967 m/day. As shown in Figure 1a, the elevation of the water table of Ordovician limestone aquifer is −38 m to −50 m. The thickness of the impermeable layer between the No. 1 coal seam and Taiyuan Formation limestone aquifers is 10.3–25.1 m, with an average of 16.2 m.

On 25 May 2017, a water inrush accident occurred on the 12,123 rock connection roadway, resulting from the concealed KCC with access to the Ordovician limestone

aquifers, and the maximum water inrush reached 14,520 m^3/h. The location of the water inrush point is shown in Figure 1.

3. Theoretical Analysis of Floor Failure

According to the stress distribution of floor rock mass, the section along the inclined direction of rock strata can be selected as the research block [22,23]. According to the Saint Venant principle, the force system acting on a local area of the elastic surface can be replaced by the equivalent static force system. In general, obvious changes in stress distribution only appear near the load, whereas the effect is small when far away from the load. Therefore, the stress distribution along the inclined direction of rock strata can be expressed by an equivalent mechanical model, as shown in Figure 2. In the figure, the action length of equivalent stress is twice the distance from the roadway boundary to the peak stress, and it can be calculated as follows:

$$l = 2x_0, \tag{1}$$

where l is the action length of equivalent stress (m), and x_0 is the distance from the roadway boundary to the peak stress (m).
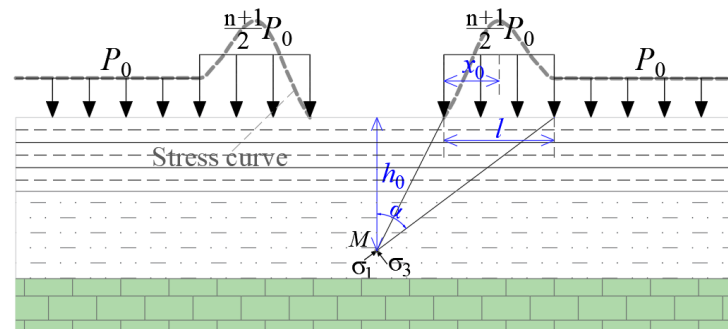

Figure 2. The sketch map of floor load along rock strata oblique section.

Considering the stress generated by the self-weight of the rock mass in the floor and the plane strain, the principal stress at any point in the floor rock can be expressed as

$$\begin{cases} \sigma_1 = \frac{q}{\pi}(\alpha + \sin\alpha) + \gamma H_0 \\ \sigma_2 = \lambda(\sigma_1 + \sigma_3) = \frac{2q\lambda\alpha}{\pi} + 2\lambda\gamma H_0, \\ \sigma_3 = \frac{q}{\pi}(\alpha - \sin\alpha) + \gamma H_0 \end{cases} \tag{2}$$

where σ_1, σ_2, and σ_3 are the maximum, intermediate, and minimum principal stresses, respectively (MPa), H_0 is the mining depth (m), γ is the rock bulk density (kg/m^3), α is the angle in Figure 2 (°), γ is the rock bulk density (kg/m^3), and q is the equivalent stress, which can be expressed as

$$q = \frac{n+1}{2} P_0, \tag{3}$$

where n is the maximum stress concentration factor, which can be obtained by field measurement (generally 2.0–3.0), and P_0 is the initial stress (MPa).

According to the Mohr–Coulomb failure criterion, the maximum failure depth of floor rock stratum caused by roadway excavation can be calculated by the following equation:

$$h_m = \frac{(n+1)P_0}{2\pi\gamma}\left(\frac{2\sqrt{\frac{1+\sin\varphi}{1-\sin\varphi}}}{\frac{1+\sin\varphi}{1-\sin\varphi}-1} - \cos^{-1}\frac{\frac{1+\sin\varphi}{1-\sin\varphi}-1}{\frac{1+\sin\varphi}{1-\sin\varphi}+1}\right) - \frac{\sigma_c}{\gamma\left(\frac{1+\sin\varphi}{1-\sin\varphi}-1\right)}, \tag{4}$$

where h_m is the floor failure depth (m), and σ_c is the uniaxial compressive strength of the rock mass (MPa).

When the initial stress $P_0 = \gamma H_0$, and $K = (1 + \sin \varphi)/(1 - \sin \varphi)$, Equation (4) can be rewritten as

$$h_m = \frac{(n+1)H_0}{2\pi}\left(\frac{2\sqrt{K}}{K-1} - \cos^{-1}\frac{K-1}{K+1}\right) - \frac{\sigma_c}{\gamma(K-1)}.$$ (5)

It can be seen that the maximum failure depth of the floor rock increases with the increase in mining depth and abutment pressure, but decreases with the increase in rock strength.

4. Mechanical Analysis of Water Inrush

The distance between the floor of the 12,123 connection roadway and the top of the collapse column is about 25 m in the PanEr Coal Mine. The rupture of the water-resisting strata between the roadway floor and the collapse column formed the water inrush channel, leading to water inrush accidents. When the roadway was excavated to 109 m, shear failure was prone to occur around the end cap due to the development and extension of the inherent structural cracks, and the shear surface was located on the vertical surface, which was approximately perpendicular to the bottom plate along the wall.

As shown in Figure 3, taking the concealed collapse column as an example, when the floor cap formed a shear surface, and the total shear force and shear resistance force on the vertical shear surface reached the ultimate equilibrium state, the total shear force on the bottom of the concealed collapse column cap could be calculated as follows:

$$F = \pi r^2 (p_w + Q - W),$$ (6)

where r is the radius of collapse column (m), p_w is the groundwater pressure (MPa), Q is the mine pressure (MPa), and W is the self-weight of the overlying strata (MPa).
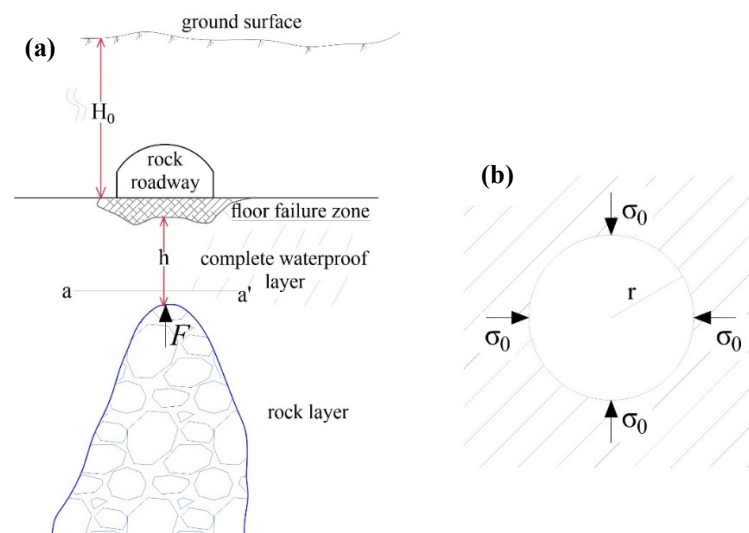
Figure 3. Water bursting mode schematic diagram of collapse column: (**a**) profile of roadway and KCC; (**b**) force diagram of a–a' section.

The shear force (f) of unit length around the collapse column boundary is expressed as

$$f = \frac{F}{2\pi r} = \frac{r}{2}(p_w + Q - W).$$ (7)

The shear resistance (τ) per unit length on the shear plane is expressed as

$$\tau = h(\sigma_0 \tan \varphi + c),$$ (8)

where h is thickness of effective water-resisting layer of the floor, σ_0 is the normal stress on the vertical shear plane (MPa), and c is the cohesion force (MPa).

It is assumed that there is a linear relationship between the dead weight stress and the buried depth of rock mass, which is determined by the thickness of overlying rock mass and key stratum.

$$\sigma_0 = \left(H_0\gamma_d + \frac{\gamma_g}{h} \int_0^h hdh \right) v = \left(H_0\gamma_d + \frac{h\gamma_g}{2} \right) v. \tag{9}$$

Substituting Equation (9) into Equation (8) yields

$$\tau = h\left[\left(H_0\gamma_d + \frac{h\gamma_g}{2} \right) v + c \right] = \frac{1}{2}h^2\gamma_g v \tan\theta + (H_0\gamma_d\tan\varphi + c)h, \tag{10}$$

where γ_d is the dry specific gravity of roof rock mass (kN/m^3), γ_g is the volume mass of rock mass (kN/m^3), v is the lateral pressure coefficient, and H_0 is the vertical depth of the roadway roof (m).

When the total shear force and shear resistance on the shear plane reach a limit equilibrium ($f = \tau$), the limited value of groundwater pressure can be obtained as follows:

$$P_w = \frac{1}{r}h^2\gamma_g v \tan\theta + \frac{1}{2}(H_0\gamma_d v \tan\varphi + c)h - Q + W. \tag{11}$$

According to the above equation, the relationship between the critical value of water pressure and the thickness of the floor cap is a quadratic parabola equation when the cap of cylindrical collapse column is damaged by shear force.

The ground elevation of the 12,123 rock connection roadway is 21.5 m, the buried depth of the roadway is 490.0–506.5 m, and the roadway is 4.0 m wide. On the basis of the analysis of a large number of floor failure depth data, the theoretical empirical formula of roadway floor failure depth can be summarized as follows:

$$h_1 = 0.7007 + 0.1079L, \tag{12}$$

where h_1 is the depth of the floor mining-induced water-conducting failure zone (m), and L is the width of the roadway or inclined length of the stope (m).

The calculated failure depth of the floor is 1.13 m. The results of borehole exploration and theoretical analysis showed that the radius of the KCC is 16.5 m, the vertical distance between collapse column top and roadway floor is 25 m, and the effective thickness of the water-resisting layer is 18.93 m. The laboratory test and monitoring results showed that the average volumetric weight of the overburden is 26 kN/m^3, the average volumetric weight of the floor stratum is 23 kN/m^3, the lateral pressure coefficient is 0.33, the empirical cohesion force of the floor layer is 0.6 MPa, and the internal friction angle is 35°. The value of the mine concentration pressure caused by excavating the roadway is 17.25 MPa. The calculated limited value of water pressure is 2.79 MPa, which is far less than the actual water pressure value of 4.71 MPa. Thus, this water inrush accident from the concealed collapse column was inevitable.

5. Water-Conducting Seepage Development of KCC

RFPA^{2D} is a numerical simulation software that is able to simulate the large movement and rotation of rock mass [24–27]. The RFPA^{2D}-Flow seepage module can be used to analyze the activated water conductivity of collapse column during roadway excavation. The dynamic development of rock cracks between the collapse column and roadway floor, and the permeability and stress evolution law during the development to expansion were simulated and analyzed. The seepage–stress coupling method was based on the following assumptions:

- The seepage process conformed to the modified Terzaghi effective stress principle;

- The elastic damage theory was used to describe the mechanical behavior of the rock medium with residual strength, and the threshold conditions of the damage process were determined according to the Mohr–Coulomb criterion;
- The material satisfied the relationship of stress–strain permeability coefficient in the elastic state, and the permeability coefficient increased obviously after being damaged;
- Considering the heterogeneity of rock materials, the physical parameters of mesoscopic units were assigned according to a certain Weibull distribution.

5.1. Seepage and Damage Coupling Equation

When the state of the mesoscopic element composed of rock material is at the given damage threshold condition, the mesoscopic element starts to calculate the damage, and the elastic modulus of the damage element can be expressed as follows:

$$E = (1 - D)E_0, \tag{13}$$

where D is the damage variable, and E_0 and E represent the elastic modulus of the undamaged element and damaged element respectively (MPa).

In the case of uniaxial compression, the failure criterion of the element body adopts the Mohr–Coulomb damage threshold and can be expressed as

$$F = \sigma_1 - \sigma_3 \frac{1 + \sin \varphi}{1 - \sin \varphi} \geq f_c, \tag{14}$$

where F is the force acting on the rock mass (MPa), and f_c is the uniaxial compressive strength (MPa). When the shear stress of the element reaches the damage threshold, the damage variable D is expressed as follows:

$$D = \begin{cases} 0, & \varepsilon < \varepsilon_{c0} \\ 1 - \frac{f_{cr}}{E_0 \varepsilon}, & \varepsilon \geq \varepsilon_{c0} \end{cases}, \tag{15}$$

where f_{cr} is the uniaxial compressive residual strength (MPa), ε is the residual strain, and ε_{c0} is the maximum compressive strain.

The damage causes a sharp increase in the permeability coefficient of the sample, and the description of the permeability coefficient of the unit is as follows:

$$\lambda = \begin{cases} \lambda_0 \partial^{-\beta(\sigma_1 - \partial p)}, & D = 0 \\ \xi \lambda_0 \partial^{-\beta(\sigma_1 - \partial p)}, & D > 0 \end{cases}, \tag{16}$$

where λ_0 is the initial permeability coefficient, and ξ, ∂, and β are the permeability coefficient increment, pore pressure coefficient, and coupling coefficient, respectively.

5.2. Numerical Simulation Analysis

The water inrush accident resulting from the concealed collapse column occurred in the 12,123 rock connection roadway, and the elevation of the water inrush point was -470 m. Collapse columns developed from the Ordovician limestone strata to the C_3^{3up} limestone floor in the Carboniferous Taiyuan Formation.

The established numerical model was 180 m in length and 250 m in height, consisting of 36,750 squares (grids 1 m × 1 m in size). The overburden weight was treated as a uniformly distributed load, which was exposed on the top of the model, while the bottom represented the Ordovician aquifers. The confined water pressure of Ordovician limestone was transferred and loaded to the model through the boundary of the underlying aquifer at the bottom of the model, and the whole model was subjected to the combined action of dead weight stress and Ordovician limestone water pressure vertically. Both sides of the model were horizontal displacement constraint boundaries, while the bottom was a vertical displacement constraint boundary. The value of confined water pressure was 2.5 MPa,

and the fixed head boundary of 500 m high was set to simulate the Ordovician Limestone aquifers, as shown in Figure 4. The excavation step distance was set to 5.0 m.

For the selection of numerical model parameters, in order to consider the uniformity of materials and the physical and mechanical properties of each rock layer, it was necessary to assume that the units of each rock layer were homogeneous and isotropic linear elastomers, and the physical and mechanical properties parameters of each rock layer unit were subjected to a Weibull distribution. The coefficient of homogeneity m was introduced to represent the uniformity of materials, which is proportional to the uniformity, i.e., a greater value of m indicates a more uniform rock material. The uniformity coefficient of this simulation was $m = 3.0$. The selection of the elastic modulus and rock mass strength was preliminarily confirmed according to the following fitting formula:

$$\frac{f_{cs}}{f_{cs0}} = 0.2602 \ln m + 0.0233, \ 1.2 \leq m \leq 50, \tag{17}$$

$$\frac{E_s}{E_{s0}} = 0.1412 \ln m + 0.6476, \ 1.2 \leq m \leq 10, \tag{18}$$

where m is the coefficient of homogeneity, E_{so} is the calculation of the input elastic modulus, f_{cso} is the calculation of the mean value of input intensity, E_s is the measured elastic modulus value, and f_{cs} is the mean value of measured intensity.
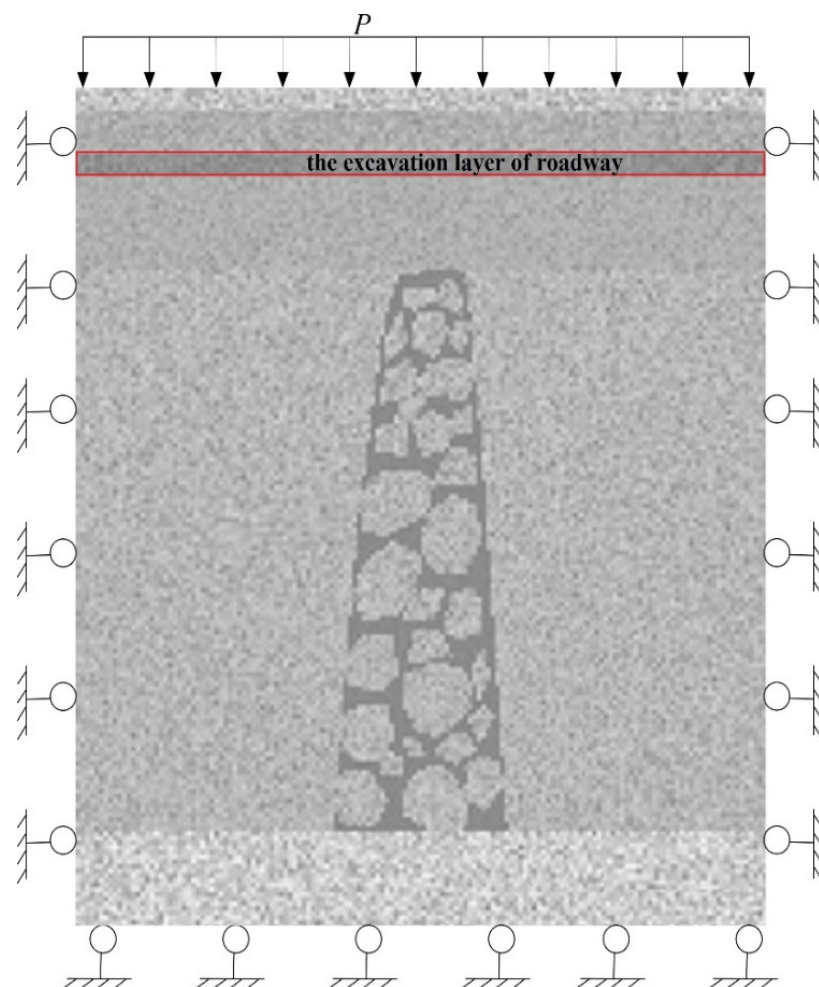


Figure 4. Schematic diagram of numeric model.

According to the indoor test results, the properties and mechanical parameters of each rock layer were determined as shown in Table 1.

Table 1. Properties and mechanical parameters of each rock layer in the RFPA model.

Stratum		Elastic Modulus (GPa)	Compressive Strength (GPa)	Fraction Angle (°)	Poisson Ratio	Volumetric Weight (kg·m⁻⁶)	Permeability Coefficient (m/D)	Water Pressure Coefficient
Overlying layer		35	0.2	35	0.3	2.50×10^{-5}	5	0.2
Roadway layer		15	0.08	38	0.35	1.80×10^{-5}	0.0005	0.15
Floor layer		35	0.15	30	0.25	2.50×10^{-5}	0.0008	0.1
KCC	Rock	40	0.17	35	0.3	2.67×10^{-5}	10	0.3
	Filling	10	0.14	15	0.35	2.50×10^{-5}	0.08	0.1
Impermeable layer		40	0.18	35	0.3	2.50×10^{-5}	0.08	0.2
Aquifer		55	0.6	38	0.25	2.50×10^{-5}	60	0.2

As shown in Figure 5, the stress of the element was released due to fracture development, and the color of the element turned black. The change process of the micro-fracture with time could be judged. Acoustic emission model arithmetic was performed on the basis of the acoustic emission energy figure at every step; the red model represents the current caused by the tensile damage acoustic emission, the white model calculation represents the current caused by shear damage acoustic emission, and the black model represents the accumulated acoustic emission.

Stress				
Acoustic emission				
Rlow field				
Excavation length	60 m	88 m	100 m	108 m
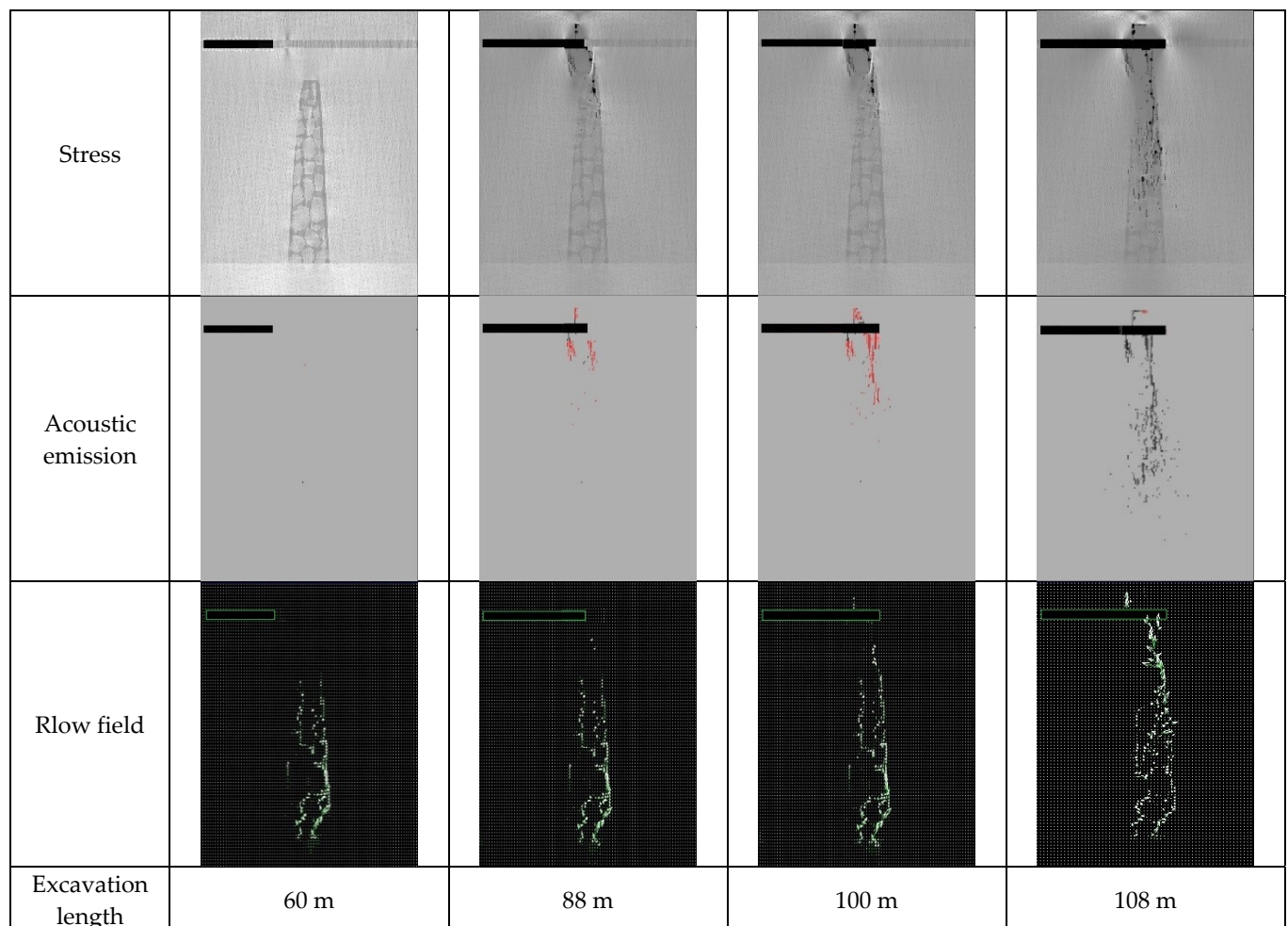
Figure 5. Numerical simulation results by RFPA during roadway extraction.

As shown in Figure 5, when the excavation length of the roadway reached 60 m, the initial stress state of surrounding rock was disturbed, which caused the stress redistribu-

tion of surrounding rock. Under the combined action of the overburden stress and the Ordovician limestone water pressure at the bottom, the stress concentration appeared in the front and rear of the excavation area. Although the pieces and fillers in the collapse column did not rush out and remained relatively stable, the confined water in the interior of the column continuously flowed upward due to the structural fragmentation.

When the roadway was excavated to 88 m, the aquiclude under the roadway floor generated obvious mining-induced fractures. These fractures were well developed and had the tendency of continuous expansion, which provided conditions for the formation of the water inrush channel.

When the roadway was excavated to 100 m, the range of mining-induced fractures continued to expand. The water pressure in the interior of the collapse column increased, and the structural fracture zone was in the state of erosion and dissolution. The filling mudstone and sand were activated by the high-pressure groundwater and were in a slow-flow state. The pores continued to increase, forming crack channels, and the water flow in the column continued to increase.

When the roadway was excavated to 108 m, the column strength decreased continuously due to the increased activation of the cracks in the roadway floor and the development of cracks in the column. Meanwhile, the filling materials were gradually washed out. With the continuous expansion of the primary fracture, a large number of secondary fractures were initiated, resulting in the accelerated upward flow of the column, which had a flushing and expansion effect on the fracture surface. When the mining-induced fractures connected with the water-conducting fractures of the collapse column, a water inrush channel similar to a pipe was formed.

6. Discussion

The gradual development process of water inrush was analyzed from the aspect of fluid–solid coupling through numerical simulation. Due to the influence of high-pressure water seepage and scouring in the rock mass of collapse column, the cracks in the rock mass expanded and the filling materials dissolved until all the cracks were connected [28,29]. Meanwhile, the flow of water inrush was transformed from pore flow to fracture flow, and finally to pipeline flow, which was manifested in a gradual increase in water inrush with a certain lag. The degree of lagging water inrush was mainly affected by the development of the collapse column, the water pressure of confine aquifers, and the growth of rock fractures disturbed by excavation.

According to the variation of inrushing water volume from the concealed KCC, the water inrush showed gradual development and could be divided into three stages, as shown in Figure 6a. In the first stage, the water yield with 15 m^3/h was originally generated at 8:00 p.m. on 23 May and then gradually increased to 90 m^3/h at 7:00 p.m. on 24 May. This stage lasted about 23 h, and the water inflow was relatively small. This was a small water inrush event that would not cause a safety threat to roadway excavation. In the second stage, the water yield increased to 280 m^3/h from 7:00 p.m. on 24 May to 8:00 p.m. on 25 May. Compared with the first stage, the water inflow increased significantly, representing a medium water inrush event. The third stage was from 8:00 p.m. to 11:00 p.m. on 25 May, which lasted only 1 h. However, the water inflow suddenly increased to about 3024 m^3/h and then to 14,520 m^3/h, presenting a sudden change state. The mine drainage facilities could not pump the water inrush into the ground in a timely manner, eventually leading to the mine flooding.

Furthermore, there were three ground holes monitoring the water level of the Ordovician limestone aquifers, namely, the Water II-1 hole, V East-O_2 hole, and VI West-O_2 hole. The dynamic changes in groundwater level during water inrush from the roadway floor were monitored as shown in Figure 6b–d. As shown in the figure, the overall trend of groundwater level in the Ordovician limestone aquifer was relatively stable with no obvious decrease before 11:00 p.m. on 25 May. After that, the water level of V East-O_2 and VI West-O_2 observation holes decreased sharply, becoming 57.97 m and 43.67 m lower

than the original water level, respectively. Then, the water level continued to decrease. Due to the good intraformational recharge of the Ordovician limestone aquifer, the water level of Water II-1 did not decrease significantly before 12:00 p.m. on 26 May; however, subsequently, the water level decreased significantly. Corresponding to the development process of water inrush, the water level of Ordovician limestone aquifers also showed the characteristics of stage decline. The water level was relatively stable in the first and second stages. The water level showed a significant decline and a longer duration in the third stage.
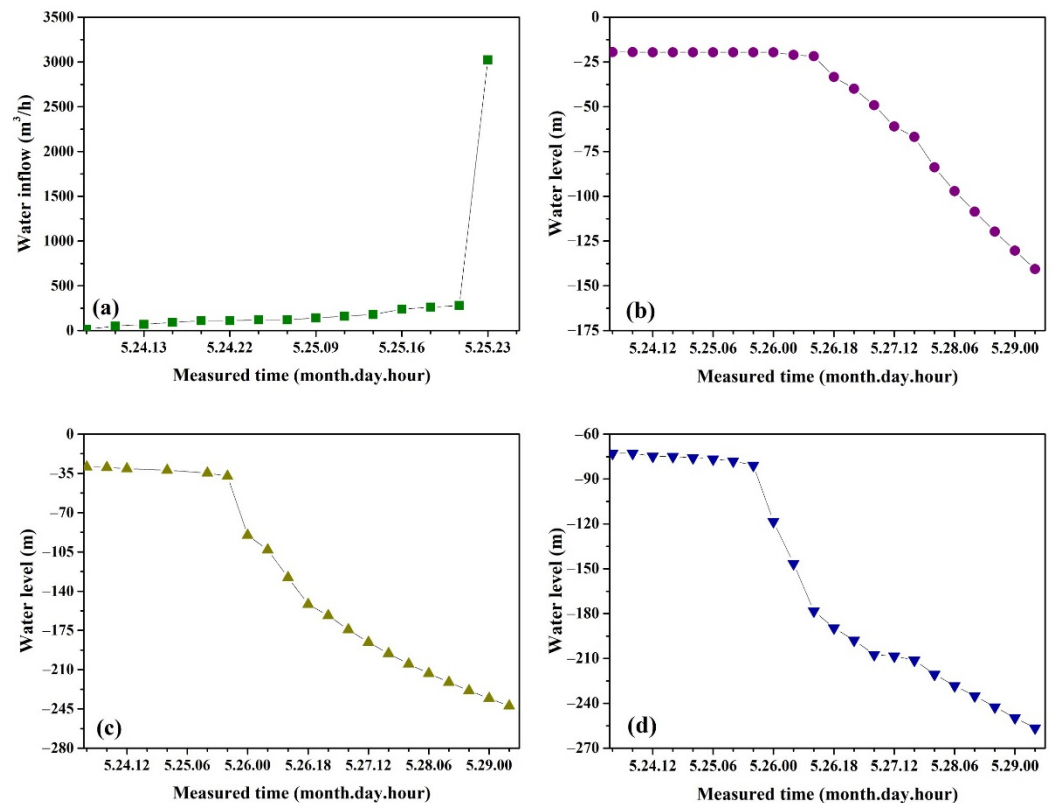
Figure 6. Curve map of water inflow and water level of the Ordovician limestone aquifers. (**a**) water inflow; (**b**) water level of Water II-1 hole; (**c**) water level of VI West-O$_2$ hole; (**d**) water level of VI West-O$_2$ hole.

The comprehensive analysis results of water inrush yield and aquifer water level change showed that the water inrush from the collapse column had obvious stage characteristics, which is consistent with the numerical simulation results. In the first stage, the floor rock mass was unloaded due to the continuous construction of the roadway. Then, the collapse column was in an unstable state, resulting in water inrush accidents under the action of high water pressure of the Ordovician limestone aquifer. However, the structure of the KCC was not destroyed entirely at this moment. This was the seepage stage, and the flow rate could be evaluated by Darcy's law. As the seepage continued, the fine particles of the column body were carried out, and the structure was destroyed in the second stage. The micro-cracks were integrated and became water inrush cracks, and the water flow presented a turbulent state. The Darcy law could no longer be used to estimate the flow rate, instead being replaced by the crack flow theory. In the third stage, as the fine particles were further brought out, the large particles and even the accompanying stones were brought out. At the same time, the KCC structure was further damaged, and the characteristics of pipeline flow were presented.

7. Conclusions

In this research, the condition and development characteristic of water inrush from a KCC were analyzed, and the delayed inrush mechanism of a concealed collapse column in

a roadway floor was analyzed from the aspects of floor failure, KCC activation, and seepage transition through theoretical calculation and numerical simulation. The changes in flow rate and underground table were compared with the simulation results. The following conclusions were obtained:

1. The rock mechanical properties and excavation depth are the main factors affecting the floor failure characteristics. The floor failure depth increases with the buried depth of the roadway, but decreases with the strength of the floor rock layers.
2. The hydraulic analysis criterion of water inrush from the KCC was established and applied to the analysis of the 25 May water inrush accident. The calculated limited value of water pressure was far less than the actual water pressure, indicating that the accident was inevitable.
3. The seepage transformation from pore flow to fracture flow and pipeline flow, with a change in the internal composition structure, is the internal mechanism of the delayed water inrush from a KCC.

Author Contributions: Conceptualization, Y.L. and J.Z.; methodology and software, Y.L.; validation, Y.L. and J.Z.; data analysis, J.Z.; investigation and resources, A.Y., S.H. and Y.B.; writing—original draft preparation, Y.L. and J.Z.; writing—review and editing, Q.L.; visualization, Y.L. and S.H.; supervision, Q.L.; project administration and funding acquisition, Y.L., Q.L. and A.Y. All authors have read and agreed to the published version of the manuscript.

Institutional Review Board Statement: Not applicable.

Informed Consent Statement: Not applicable.

Data Availability Statement: Not applicable.

Conflicts of Interest: The authors declare no conflict of interest.

References

1. Wang, W.; Zhao, W.D.; Qian, J.Z.; Ma, L.; Wang, D.J.; Hou, X.L. Potential of hydraulic tomography in exploring the preferential flowpaths of water inrush in coal mine areas. *J. Hydrol.* **2021**, *602*, 126830. [CrossRef]
2. Liu, B.; Malekian, R.; Xu, J. Groundwater mixing process identification in deep mines based on hydrogeochemical property analysis. *Appl. Sci.* **2017**, *7*, 42. [CrossRef]
3. Gui, H.; Xu, J.; Zhang, D. Relationship between hydraulic conductivity of karst collapse column and its surrounding lithology. *Environ. Earth Sci.* **2017**, *76*, 215. [CrossRef]
4. Feng, F.; Peng, S.; Fu, P.; Du, W.; Xu, D. A study on the seepage flow characteristics and disaster-causing mechanism of collapse column. *Adv. Civ. Eng.* **2018**, *2018*, 7841649. [CrossRef]
5. Polak, K.; Ro'zkowski, K.; Czaja, P. Causes and effects of uncontrolled water inrush into a decommissioned mine shaft. *Mine Water Environ.* **2016**, *35*, 128–135. [CrossRef]
6. Yin, S.X.; Lian, H.Q.; Liu, D.M.; Yin, H.C. 70 years of investigation on karst collapse column in North China Coalfield: Cause of origin, mechanism and prevention. *Coal Sci. Technol.* **2019**, *47*, 1–29.
7. Zuo, J.P.; Hong, Z.J.; Peng, S.P.; Shi, Y.; Song, H.Q.; Li, M.; Zhang, Z.S. Investigation on failure behavior of collapse column in China's coal mine based on discontinuous deformation numerical method. *PLoS ONE* **2019**, *14*, e0219733. [CrossRef] [PubMed]
8. Intrieri, E.; Gigli, G.; Nocentini, M.; Lombardi, L.; Mugnai, F.; Fidolini, F.; Casagli, N. Sinkhole monitoring and early warning: An experimental and successful GB-InSAR application. *Geomorphology* **2015**, *241*, 304–314. [CrossRef]
9. Zhao, J.G.; Guo, M.T.; Li, W.S. Morphological and fabric characteristics of Karst collapse pillars in Xishan coalfield. *J. China Coal Soc.* **2020**, *45*, 2389–2398.
10. Zhang, H.T.; Xu, G.Q.; Zhan, H.B.; Zheng, J.B.; Wang, M.H.; Liu, M.C.; Pan, S.Q.; Wang, N. Formation mechanisms of paleokarst and karst collapse columns of the middle Cambrian-lower Ordovician carbonates in Huainan coalfield, Northern China. *J. Hydrol.* **2021**, *601*, 126634. [CrossRef]

11. Yin, S.X.; Wu, Q.; Wang, S.X. Hydrogeological and mechanical basic of water inrush from karstic columns in Northern China. *J. China Coal Soc.* **2004**, *29*, 182–185.

12. Hu, B.L.; Song, X.M. Formation mechanism of deep karst caves and collapse columns in Huaibei coalfield. *Coal Geol. Chin.* **1997**, *9*, 45–47.

13. Qian, X.P. The formation of gypsum karst collapse column and its hydrogeological significance. *IAHS-AISH Publ.* **1988**, *176*, 1186–1193.

14. Hou, E.K.; Xia, Y.C.; Fan, H.R.; Ju, T.Y. Cause analysis and prediction of mine collapse column. *Northwest. Geol.* **1944**, *15*, 18–22.

15. Si, S.P.; Ma, J.M.; Hu, D.X. The Origin mechanism and distribution regularity of karst collapse in coal measure strata. *Fault-Block Oil Gas Field* **2001**, *8*, 15–18+66.

16. Cao, Z.Z.; Ren, Y.L.; Wang, Q.T.; Yao, B.H.; Zhang, X.C. Evolution mechanism of water-conducting channel of collapse column in karst mining area of Southwest China. *Geofluids* **2021**, *2021*, 6630462. [CrossRef]

17. Ma, D.; Wang, J.J.; Li, Z.H. Effect of particle erosion on mining-induced water inrush hazard of karst collapse pillar. *Environ. Sci. Pollut.* **2019**, *26*, 19719–19728. [CrossRef]

18. Jiang, Y.L.; Zhang, D.F.; Wang, K.; Zhang, X.Q. Mining-Induced Damage Characteristics of Floors during Fully Mechanized Caving Mining: A Case Study. *Adv. Mater. Sci. Eng.* **2018**, *2018*, 1513451. [CrossRef]

19. Tang, C.A.; Tham, L.G.; Lee, P.K.K.; Yang, T.H.; Li, L.C. Coupled analysis of flow, stress and damage (FSD) in rock failure. *Int. J. Rock Mech. Min.* **2002**, *39*, 477–489. [CrossRef]

20. Li, W.P.; Liu, Q.M.; Sun, R.H. Theoretical and experiment study on vadose conversion of water inrush later occurred from structure broken zone. *Coal Sci. Technol.* **2011**, *39*, 10–13.

21. Li, G.Y.; Zhou, W.F. Impact of karst water on coal mining in North China. *Environ. Geol.* **2006**, *49*, 449–457. [CrossRef]

22. Xu, Z.M.; Sun, Y.J.; Gao, S.; Chen, H.Y.; Yao, M.H.; Li, X. Comprehensive exploration, safety evaluation and grouting of karst collapse columns in the Yangjian coalmine of the Shanxi province, China. *Carbonates Evaporites* **2021**, *36*, 16. [CrossRef]

23. Lai, X.P.; Xu, H.C.; Shan, P.F.; Kang, Y.L.; Wang, Z.Y.; Wu, X. Research on mechanism and control of floor heave of mining-influenced roadway in top coal caving working face. *Energies* **2020**, *13*, 381. [CrossRef]

24. Deng, X.F.; Zhu, J.B.; Chen, S.G.; Zhao, J. Some Fundamental Issues and Verification of 3DEC in Modeling Wave Propagation in Jointed Rock Masses. *Rock Mech. Rock Eng.* **2012**, *45*, 943–951. [CrossRef]

25. Wu, J.H.; Lin, W.K.; Hu, H.T. Assessing the impacts of a large slope failure using 3DEC: The Chiu-fen-erh-shan residual slope. *Comput. Geotech.* **2017**, *88*, 32–45. [CrossRef]

26. Liu, B.; He, K.; Han, M.; Hu, X.W.; Wu, T.W.; Wu, M.Y.; Ma, G.T. Dynamic process simulation of the Xiaogangjian rockslide occurred in shattered mountain based on 3DEC and DFN. *Comput. Geotech.* **2021**, *134*, 104122. [CrossRef]

27. Ge, Y.F.; Tang, H.M.; Li, C.D. Mechanical energy evolution in the propagation of rock avalanches using field survey and numerical simulation. *Landslides* **2021**, *18*, 3559–3576. [CrossRef]

28. Kong, H.; Wang, L. Seepage problems on fractured rock accompanying with mass loss during excavation in coal mines with karst collapse columns. *Arab. J. Geosci.* **2018**, *11*, 585. [CrossRef]

29. Lin, Z.B.; Zhang, B.Y.; Gong, X.F.; Sun, L.M.; Wang, W.Z.; Yang, D.F.; Yang, Y.L.; Guo, M.; Pan, X.H. Analysis and application of the mechanical properties of the karst collapse column fillings. *Shock Vib.* **2021**, *2021*, 5519048. [CrossRef]